Electronic Supplementary Material (ESI) for Chemical Communications.
This journal is © The Royal Society of Chemistry 2016

Supporting Information

Breakthrough in Concentration Quenching Threshold of Upconversion Luminescence via spatial separation of emitter doping area for Bio-application

Xiaomin Liu[a], Youlin Zhang[a], Langping Tu[a], Yu Wang[b], Qinghui Zeng[a], Chunguang Li[c], Zhan Shi[c], Xianggui Kong[a]* and Hong Zhang[b]*

[a]Changchun Institute of Optics, Fine Mechanics and Physics, Chinese Academy of Sciences, P. R. China. *e-mail:xgkong14@ciomp.ac.cn

[b]Van't Hoff Institute for Molecular Sciences, University of Amsterdam, The Netherlands. *e-mail:h.zhang@uva.nl

[c]State Key Laboratory of Inorganic Synthesis & Preparative Chemistry, College of Chemistry, Jilin University, P. R. China.

18th August 2016

Note added after first publication: This Supplementary Information file replaces that originally published on 4th October 2011, and contains a corrected image for Fig. S5.

Contents:

(6) Fig. S6. Evidence for sandwich structure of model A.

(7) Fig. S7. UC PL spectra of model C doped with various concentration of Er^{3+} ions.

(8) Fig. S8. The further explanation for the spectral difference related to Figure 2.

(9) Fig. S9. EDS spectra of model A doped with 2%, 5% and 10% Er^{3+} ions.

(10) Fig. S10. Details of UCP-RB nanoconjugates.

(11) Fig. S11. The FTIR spectrum of nanoparticles after ligand exchange process.

Part 1: Experiment section

(1) Nanoparticle Synthesis: Nanoparticles of these three different models were all synthesized using a four-step process. First, the core precursors dissolved in a small amount of oleic amine were injected using a mechanical pump into the reaction vessel containing only the coordinating oleic amine ligand and non-coordinating solvent 1-octadecene. Upon formation of the core nanoparticles, the other three shell precursors were also mechanically injected into the reaction flask step by step resulting in the final hexagonal-phase nanoparticles.

CF_3COONa, $Y(CF_3COO)_3$, $Er(CF_3COO)_3$ and $Yb(CF_3COO)_3$ were purchased form GFS chemicals; Oleylamine (OM), Poly(allylamine), Rose Bengal (RB), 6-bromohexanoic acid, N-hydroxy succinimide (NHS), 1-ethyl-3-(3-dimethyllaminopropyl) carbodiimide (EDC) were purchased form Aldrich; 3-diphenylisobenzofuran (DPBF) was purchased form Fluka and all of them used without further purification.

Take the $NaYF_4$: Er^{3+} 2%, Yb^{3+} 20%/ $NaYF_4$: Yb^{3+} 20% /$NaYF_4$: Er^{3+} 2%, Yb^{3+} 20%/ $NaYF_4$: Yb^{3+} 20% for example.

The precursors used for the preparation of the core and the illuminated shell ($NaYF_4$: Er^{3+} 2%, Yb^{3+} 20%) were prepared by mixing 0.272g CF_3COONa, 0.376g $Y(CF_3COO)_3$, 0.113g $Yb(CF_3COO)_3$ and 0.011g $Er(CF_3COO)_3$ with 10mL OM. Then the slurry was heated to 100 °C to remove water and oxygen, with vigorous magnetic

stirring under vacuum for 30 min in a temperature-controlled electromantle, and thus to form a transparent solution A.

The precursors used in the preparation of the active shell ($NaYF_4$: Yb^{3+} 20%) were prepared by mixing 0.272g CF_3COONa, 0.376g $Y(CF_3COO)_3$ and 0.126g $Yb(CF_3COO)_3$ with 10mL OM. Then the slurry was also heated to 100 °C to remove water and oxygen, with vigorous magnetic stirring under vacuum for 30 min in a temperature-controlled electromantle, and thus to form a transparent solution B.

1) ***Detailed Synthesis of model A***

Step 1: The core was prepared by adding 3 mL core precursors (solution A) to the reaction vessel (three-necked Flask), which was placed under Ar gas and the temperature was slowly raised, at a rate of approximately 10 °C /min, to 320 °C. The solution was maintained at this temperature and stirred vigorously for 60 min to form the $NaYF_4$:Er^{3+} 2%, Yb^{3+} 20% core.

Step 2: The solution was then allowed to cool to 50 °C, when 5 mL of the shell precursors (Solution B) were mechanically injected (at a rate of 0.5 ml/min) into the reaction vessel containing the core nanoparticles. After that, the temperature was slowly raised to 320 °C at a rate of approximately 10 °C /min and the solution was maintained at this temperature and stirred vigorously for 30 min to form the separated shell.

Step 3: Again, 8 mL of the illuminated shell precursors (Solution A) were mechanically injected (at a rate of 0.5 ml/min) into the reaction vessel when the previous solution was cooling to 50 °C. After that, the temperature was slowly raised to 320 °C at a rate of approximately 10 °C /min and the solution was maintained at this temperature and stirred vigorously for 30 min to form the second illuminated shell.

Step 4: Repeat step 2 to form the final active shell, except that 12 mL of the shell precursors (Solution B) were mechanically injected (at a rate of 0.5 ml/min) into the reaction vessel. When the reaction was completed, an excessive amount of ethanol was poured into the solution at room temperature. The resultant mixture was

centrifugally separated, and the products were collected. The as-precipitated nanocrystals were washed several times with ethanol and dried in air at 70 °C overnight. The as-prepared nanocrystals could be easily redispersed in various nonpolar organic solvents such as hexane, toluene, and chloroform.

2) ***Detailed Synthesis of model B***

In the case of model B, the nanoparticles are synthesized by mixing the lanthanide trifluoroacetate precursors of the first three steps of model A, gradually forming a bigger core as the same size as the first three parts in model A, keeping the final active shell the same. In details, the bigger core was prepared by three steps, the same way as that used to synthesize the first three parts of model A, except that the precursors for all these three steps were prepared by adding 3 mL core precursors (solution A), 5 mL separating shell precursors (Solution B) and 8 mL illuminating shell precursors (Solution A) together. After forming the bigger core, the active shell was prepared in the same way as step 4.

3) ***Detailed Synthesis of model C***

The synthetic procedure of model C was the same as that used to synthesize model A, except that in step 2, we use 5 mL of the precursor solution A instead of solution B.

(2) Phase transfer: The ligand exchange process was carried out to transfer hydrophobic upconversion nanoparticles into hydrophilic ones using Poly(allylamine) as ligand. 0.1ml of Poly(allylamine) 20% solution in water was dispersed in 10 ml ethanol, The hydrophobic UCNPs solution (~5mg, purified and dispersed in 2ml of cyclohexane) were mixed with the Poly(allylamine) solution and stirred vigorously over 48 h at 30 °C. After centrifugation, the obtained nanoparticles were redispersed in water. After phase transfer, the Poly(allylamine) terminated UCP give amino group (see Fig. S11) at the end which can be used for covalently coupling with carboxyl ended molecules.

(3) UCP-RB conjugates: Hexanoic acid ester of Rose Bengal (RB-HA) was first gained by reacting with 6-bromohexanoic acid, and then NHS ester of RB-HA was synthesized as described in a previous protocol.[1] $NaYF_4$: Yb,Er 2.5 mg/ml solution was incubated with 1mg RB-HA-NHS at room temperature for 4 hours. UCP-RB conjugates were dialyzed in water for two days to remove unreacted photosensitizer.

(4) Singlet oxygen detection: $^1O_2$ was detected chemically using DPBF as a singlet oxygen sensor. Stock solutions of UCP-RB conjugates were prepared by dispersing nanoconjugates in Water. DPBF (8 mM) solution was prepared. All were kept in the dark. The DPBF stock solution 15μL was added to a vial containing 2 mL of the photosensitizer stock solution, mixed well, and then the mixture was irradiated at 980 nm using a CW laser.

(5) Characterization: The structure and morphology of the NCs were characterized by using a Brucker D8-advance X-ray diffractometer (XRD) with Cu Ka radiation (λ = 1.5418 Å), field emission scanning electron microscopy (FESEM, Hitachi, S-4800) with an energy-dispersive X-ray spectrometer (EDS). The transmission electron microscopy (TEM) was performed on a Tecnai G2 F20 S-TWIN D573 electron microscope operated at 300 kV TEM. The upconversion emission spectra were acquired using a Jobin-Yvon LabRam Raman spectrometer system equipped with 1800 and 600 grooves/mm holographic gratings, respectively, and a Peltier air-cooled CCD detector. The samples were excited under 15Wcm^{-2} continuous excitation at 980 nm diode laser. The upconversion luminescence spectra were measured under identical conditions in order to compare their relative emission intensities. The reduction in absorption was monitored as function of time after irradiating samples with 980nm diode laser using Hewlett-Packard/Agilent 8453 Diode-Array

Biochemical Analysis UV-Vis Spectrophotometer. The luminescence kinetics was recorded with a 500 MHz Tektronix digital oscilloscope and the excitation was realized by a nanosecond pulse train at 488 nm from an optical parametric oscillator.

Part 2: Supplementary figures

Figu. S1. Experimental powder X-ray diffraction (XRD) pattern for the final products (model A) and the calculated line pattern for the hexagonal $NaYF_4$ phase.

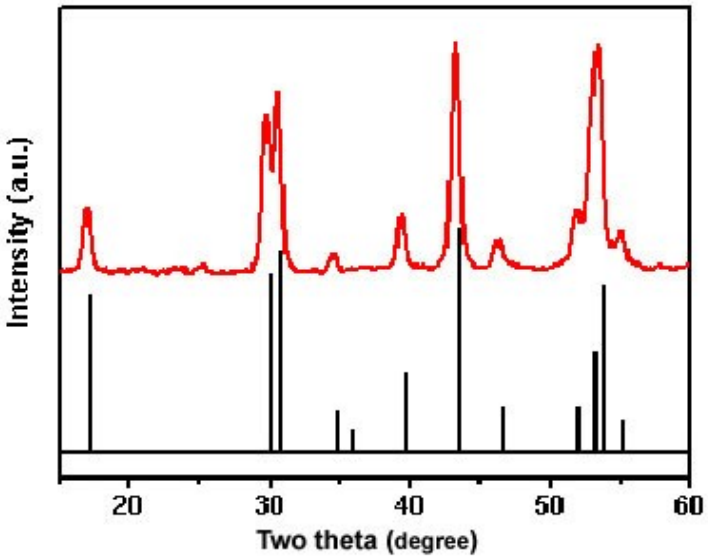

Fig. S2. Histogram of the nanoparticle size distribution showing the different states of nanoparticles (model A): a) core; b) with the separating shell outside (a); c) with the illuminating shell outside (b); d) with the final active shell outside (c).

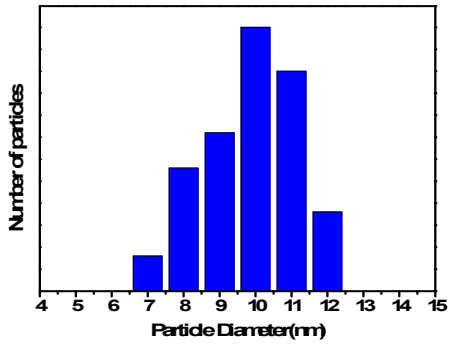

(a)

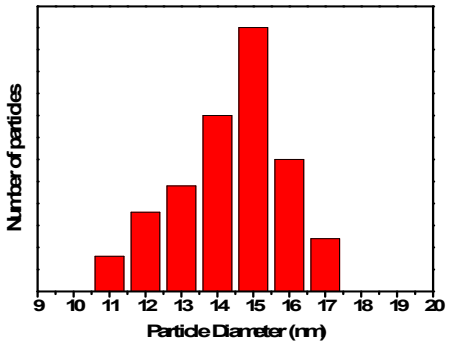

(b)

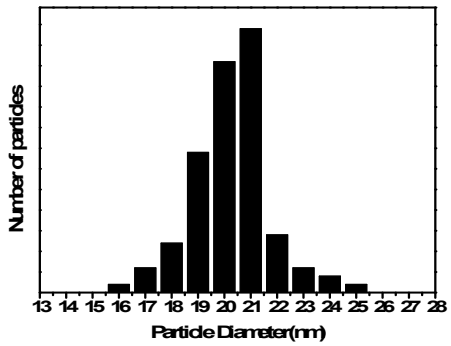

(c)

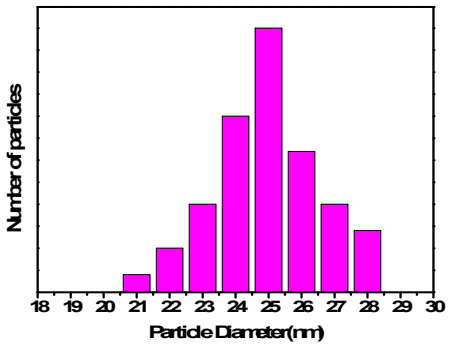

(d)

Fig. S3. TEM images of the different structured nanoparticles: a) core; b) with separating shell outside (a); c) with illuminating shell outside (b); d) with final active shell outside (c).

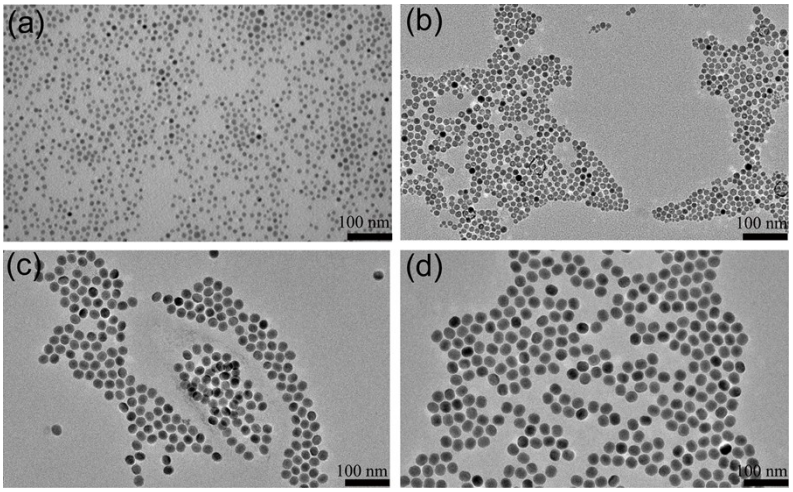

Fig. S4. Structures of models A, B and C.

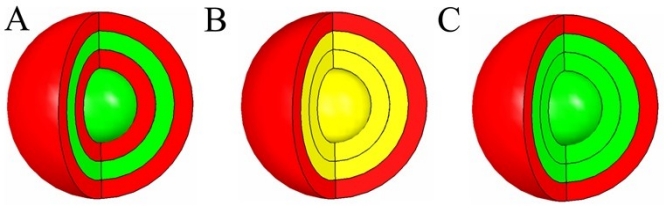

Model A contains four parts: the core ($NaYF_4$: 20% Yb, 2% Er), the first separating shell ($NaYF_4$: 20% Yb), the second illuminating shell ($NaYF_4$: 20% Yb, 2% Er) and the final active shell ($NaYF_4$: 20% Yb). Model B differs from model A by mixing the lanthanide trifluoroacetate precursors of the first three parts of model A, gradually growing the core (see Figure S4, the yellow part in model B) until reaching the same size of the first three parts in model A, keeping the final active shell unchanged. Compared with model A, model B has the same doped quantity but lower doping concentration. The Er^{3+} concentration in model A is 2%, while in mode B is 1.4%. Actually, model B is a mimic of the situation that structure of model A does not formed and emitters are homogeneously distributed due to diffusion. For model C, we doped 2% Er^{3+} into the first separating shell, also forming a core (see Figure S4, the green part in model C) as big as the first three parts of model A, and kept the final active shell the same. With this structure model C has the same doping concentration but higher doped quantity comparing to model A. To guarantee that the nanoparticles of these three different models have the same size, the amount of the lanthanide trifluoroacetate precursors of every part and the way of the synthetic approach were kept the same (see Experiment section for complete synthetic approach).

Fig. S5. TEM images of nanoparticles (models B and C).

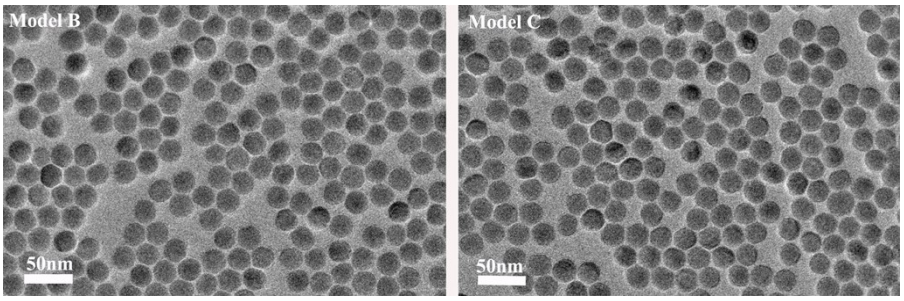

Fig. S6. UC PL spectra of colloidal nanocrystals with (1) separated model $NaYF_4$:Yb^{3+}(20%), Er^{3+}(2%) / $NaYF_4$:Yb^{3+}(20%), Tm^{3+}(0.3%) / $NaYF_4$:Yb^{3+}(20%), and (2) homogeneous model $NaYF_4$:Yb^{3+}(20%), Er^{3+}(2%), Tm^{3+}(0.3%)/ $NaYF_4$:Yb^{3+}(20%) dispersed in cyclohexane (1mg/ml) under 15Wcm^{-2} continuous excitation at 980 nm.

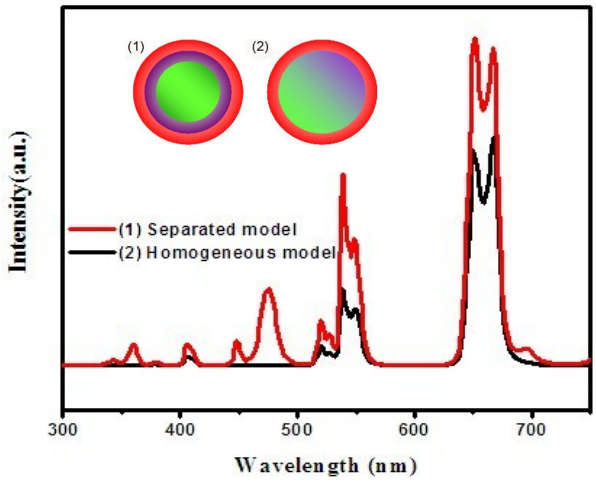

To further prove the existence of the sandwich-type architecture, we used two different emitters Er^{3+} and Tm^{3+}, and designed separated model and homogeneous model for comparison. Every shell thickness was also kept to be about 2.5 nm. The absorber Yb^{3+} ions absorb NIR light, followed by energy transfer to the emitter Er^{3+} or Tm^{3+} ions that emit visible light. For Er^{3+} and Tm^{3+} codoped nanocrystals (homogeneous model), the fluorescence from Tm^{3+} is quenched by Er^{3+}, probably as a result of the preferential energy transfer from Yb^{3+} to Er^{3+}. As such, only Er^{3+} fluorescence can be observed. While in the separated model, the Er^{3+} and Tm^{3+} fluorescence can both be clearly observed. Therefore, it is also validated the formation of sandwich structure. These results have already been reported.[2]

Fig. S7. UC PL spectra of colloidal $NaYF_4$ nanocrystals with structure of model C codoped with 20% Yb^{3+} and various concentrations of Er^{3+} ions (2%, 3% and 5%) dispersed in cyclohexane (1 mg/ml) under 15Wcm^{-2} continuous excitation at 980 nm.

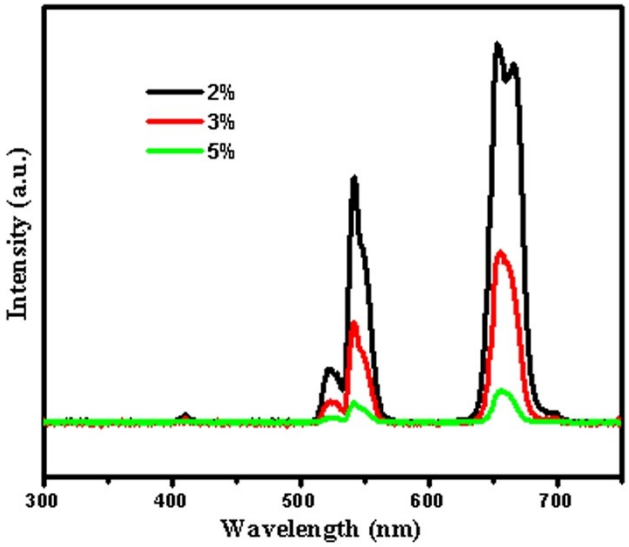

Fig. S8. The schematic illustration of the upconversion luminescence process with 980 nm excitation.

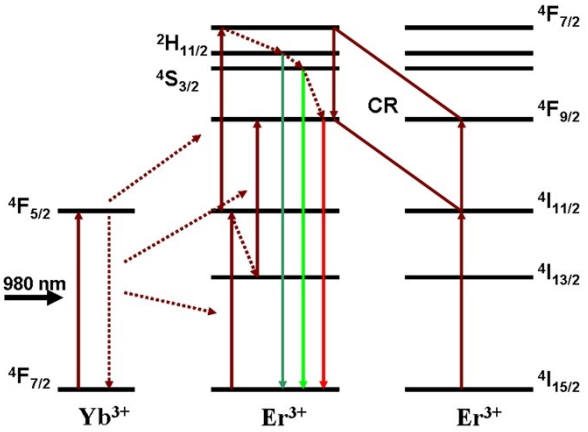

The spectral difference, especially the R/G ratio difference in Figure 2 is also related with the UC mechanism. The energy level $^4F_{9/2}$ for the red emission ($^4F_{9/2} \rightarrow {}^4I_{15/2}$) can be populated via the following processes:[2] the first one is the direct population from the $^4I_{13/2}$ level, through the non-radiative relaxation of the $^4I_{11/2}$ level, the second one is via a non-radiative relaxation from the $^4S_{3/2}$ level, and the third one is by a cross-relaxation process of $^4F_{7/2} \rightarrow {}^4F_{9/2}$ and $^4I_{11/2} \rightarrow {}^4F_{9/2}$ between the two nearby Er^{3+} ions. The first two processes emphasize the importance of multi-phonon relaxation, mainly caused by the presence of the organic groups on the surface of the nanoparticles. In the present case, the particles of these three different models are all coated with active shell and the same in size, thus we do not expect much difference in the red emission populated by the multi-phonon relaxation. The cross-relaxation, which is interrelated with the distance between two neighbouring emitters, is then the one responsible for the difference of red emission difference. From this point of view, the Er^{3+} – Er^{3+} distance in model B is less than that in model C. Therefore, the red to green (R/G) ratio of model B (R/G ratio = 1.70) is less than that of model C (R/G ratio = 2.15). As far as models A and C are concerned, they have the same Er^{3+} – Er^{3+} distance but different architectures, the red to green (R/G) ratio of model A (R/G ratio = 1.15) is less than that of model C (R/G ratio = 2.15). It is rational to imagine that in model A the sandwich-like architecture hampers the cross-relaxation process in the interface, leading to the enhancement of the overall UC luminescence and the relatively low R/G ratio.

Fig. S9. EDS spectra of the samples (model A) doped with 2%, 5% and 10% Er^{3+} ions

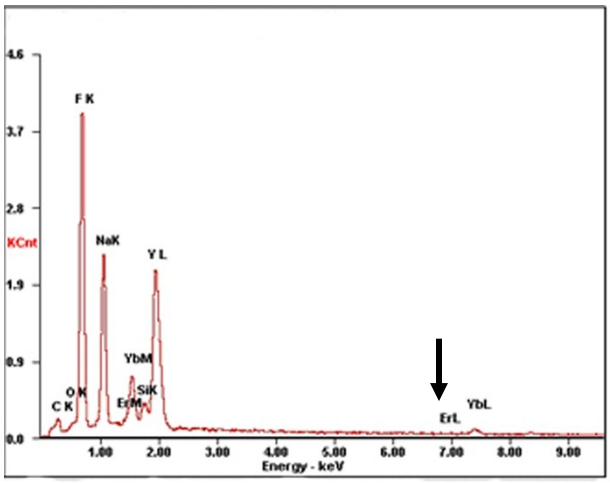

The Er^{3+} concentration was estimated to be about 0.25 atom%

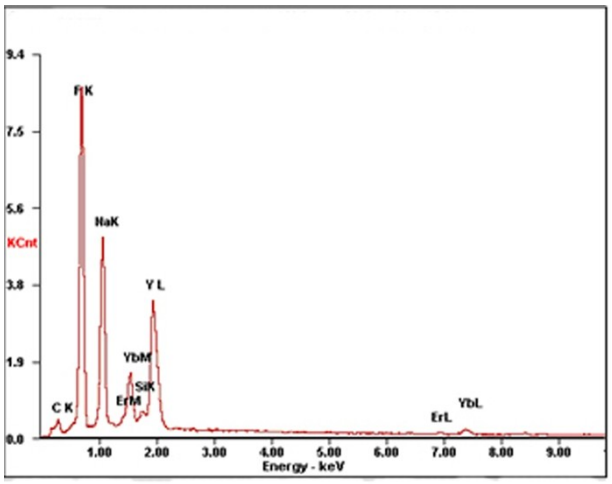

The Er^{3+} concentration was estimated to be about 0.54 atom%

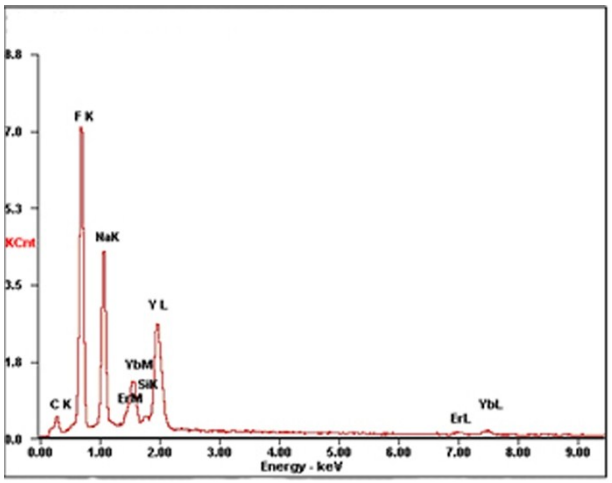

The Er^{3+} concentration was estimated to be about 1.06 atom%

Fig. S10. Schematic drawing of FRET-based $NaYF_4$-Rose Bengal (UCP-RB) nanoconjugates.

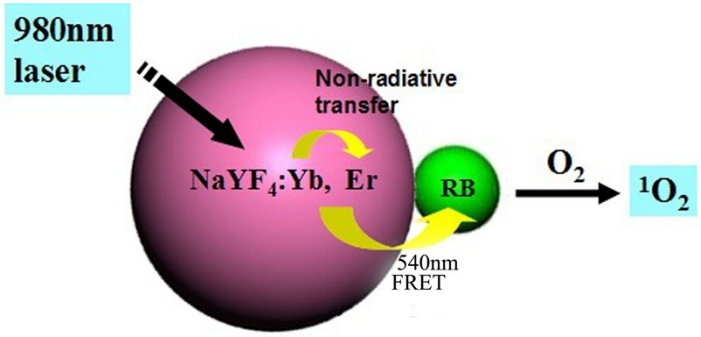

Rose Bengal is one of the clinical used photosensitizers in the cancer therapy. When the UCP-RB nanoconjugates are irradiated by infrared light, the visible UC emission from the nanoparticles will be transferred to the photosensitizing molecules coated on their surfaces based on fluorescence resonance energy transfer (FRET). Subsequently, excited photosensitizing molecules will interact with surrounding ground-state oxygen molecules, generating the very aggressive $^1O_2$ to decline the targeted cancer cells. Theoretically, the increase of UC emission should promote the singlet-oxygen generation.

Fig. S11. The FTIR spectrum of nanoparticles after ligand exchange process, illustrating the existence of amino group.